Published in final edited form as:

Nat Nanotechnol. 2019 March ; 14(3): 252–259. doi:10.1038/s41565-019-0365-6.

DNA nanodevices map enzymatic activity in organelles

Krishna Dan[1,2], **Aneesh T Veetil**[1,2], **Kasturi Chakraborty**[1,2], **Yamuna Krishnan**[1,2,*]

[1]Department of Chemistry, University of Chicago, Chicago, IL, 60637, USA

[2]Grossman Institute of neuroscience, Quantitative biology and Human Behaviour, University of Chicago, Chicago, IL 60637, USA

Abstract

Cellular reporters of enzyme activity are based on either fluorescent proteins or small molecules. Such reporters provide information corresponding to wherever inside cells the enzyme is maximally active and preclude minor populations present in sub-cellular compartments. Here we describe a chemical imaging strategy to selectively interrogate minor, sub-cellular pools of enzymatic activity. This new technology confines the detection chemistry to a designated organelle, enabling imaging of enzymatic cleavage exclusively within the organelle. We have thus quantitatively mapped disulfide reduction exclusively in endosomes in *C. elegans* and identified that exchange is mediated by minor populations of enzymes PDI-3 and TRX-1 resident in endosomes. Impeding intra-endosomal disulfide reduction by knocking down TRX-1 protects nematodes from infection by *Corynebacterium diphtheriae,* revealing the importance of this minor pool of endosomal TRX-1. TRX-1 also mediates endosomal disulfide reduction in human cells. A range of enzymatic cleavage reactions in organelles are amenable to analysis by this new reporter strategy.

Minor populations of proteins and protein complexes perform critical functions for the cell. For example, a minor population of the epidermal growth factor receptor present on exosomes mediates intercellular communication[1]. A small fraction of mammalian target of rapamycin, present on lysosomes is responsible for nutrient sensing by the cell[2]. A minor population of the KDEL receptor present in the Golgi apparatus performs the critical function of retrieving ER-resident proteins from the Golgi apparatus[3]. Small molecules that function as fluorescent reporters of enzymatic activity use highly specific and rapid

*Correspondence and requests for materials should be addressed to Y. Krishnan (yamuna@uchicago.edu).

Author Contributions

KD and YK designed the project. KD developed tripartite TDX reporters and performed all experiments related to TDX reporter in *C. elegans* and mammalian cells. ATV prepared the dextran encapsulated icosahedron and *in vitro* experiments related to icosahedron. KC contributed to cathepsin related experiments. KD, ATV, KC and YK analyzed the data. KD, ATV and YK wrote the paper. All authors discussed the results and gave input on the manuscript.

Competing financial interest. The authors do not declare any competing financial interest.

Additional Information. Supplementary information is available in the online version of the paper.

Data Availability Statement:

The data that support the plots within this paper and other finding of this study are available from the corresponding author upon reasonable request.

Reporting Summary. Further information on research design is available in the Nature Research Reporting Summary linked to this article.

detection chemistries. However, the cleaved probe molecules diffuse throughout the entire cell and thus, location-specific information on protein activity is lost[4,5]. Alternatively, genetically engineered protein tags provide spatial information[6,7], however, one can only study the major population of the protein of interest. Thus, it is extremely challenging to selectively address the activity of a minor enzyme population *in situ.* Here, using DNA nanodevices targeting to sub-cellular organelles we describe a new strategy to exclusively study the activity of a minor population of enzyme in live cells. We demonstrate proof of concept by selectively mapping enzyme-mediated disulfide reduction within endosomes, despite thiol-disulfide exchange occurring rampantly throughout the cell.

Thiol disulfide exchange occurs mainly in the cytosol, mitochondria and the endoplasmic reticulum, to correctly fold disulfide-bridged proteins[8,9]. Targeted disulfide reduction of specific proteins changes their conformation, thus triggering signalling cascades[10]. For example, disulfide reduction of C-terminal SRC kinase results in kinase activation leading to cell proliferation and cancer[11]. However, a small proportion of thiol-disulfide exchange occurs in endocytic organelles. Endosomal disulfide reduction is indispensable to degrading endocytosed proteins and pathogenic material as well as for antigen cross-presentation[12,13]. In fact, several pathogens exploit this chemistry in the endosome to infect host cells[14].

Thiol-disulfide exchange is generally studied using small molecule probes that are either cell-permeable or or do so post endocytosis[55,15]. Disulfide exchange in the cytosol then enhances probe fluorescence. While highly specific to thiol-disulfide exchange, such probes cannot report on organellar disulfide exchange. Intra-endosomal disulfide reduction was first established in cell lysates post-treatment with radio-labelled, reducible substrates as probes, analysed as a function of time[16,17]. However, spatial information is inaccessible to these biochemical methods. While responsive to small thiols such as glutathione, protein-based redox probes cannot report on enzyme catalysed disulfide reduction as the disulfide bond in the protein probe is sterically hindered[18].

DNA has proven to be a versatile and engineerable biological scaffold for quantitative imaging in living systems[19]. Functional DNA motifs such as aptamers can recognize a range of analytes, and enabled diverse sensing applications *in vitro*[20]. In fact, several detection chemistries have been deployed to ratiometrically image analytes in living systems by leveraging the precise stoichiometry of DNA hybridization to incorporate a reference fluorophore in a well-defined stoichiometry[21]. Molecular trafficking motifs can be integrated on DNA nanodevices to localize then within organelles, enabling chemical mapping[22,23]. DNA nanodevices attached to diverse endocytic ligands can target specific endocytic pathways[19]. We therefore reasoned that by integrating a fluorescent reporter sensitive to thiol-disulfide exchange onto an organelle targetable DNA nanodevice, we would be able to exclusively study endosomal disulfide reduction.

New ratiometric reporters of disulfide exchange

We created a DNA-based, ratiometric reporter consisting of three modules, each with a distinct function (Fig. 1a). The first is a sensing module, consisting of a reaction centre that fluoresces upon thiol-disulfide exchange (Fig. 1a, λ_{em} = 520 nm). The second comprises a

normalizing module, a rhodamine dye (Fig. 1a, λ_{em}= 590 nm) whose fluorescence properties are redox and ion insensitive. The third module comprises a targeting functionality, namely, a DNA duplex comprising two oligonucleotides O-Azide and O-Rhodamine Red X (SI Table 1) that serves two purposes. The first is to display the sensing and normalizing modules in a precise, 1:1 stoichiometry. The second is to target the entire assembly to the scavenger receptor-mediated endocytic pathway[24]. All three functions are integrated with stoichiometric precision by hybridizing DNA strands bearing each of these functionalities.

The working principle of the sensing module of the disulfide exchange reporter comprises a fluorescein derivative whose fluorescence is caged using carbonate linker (Fig. 1b)[4]. The other end of the carbonate linker bears a thiopyridyl group via a disulfide bond (Fig.1b, SI scheme 1). Disulfide reduction results in the deprotection of the fluorescein moiety leading to high fluorescence at 520 nm.

To make a quantitative reporter system for disulfide reduction suited to the high autofluorescence encountered *in vivo,* we made two more nanodevices. One of these, TDX_{ON}, comprises the DNA duplex attached to fluorescein (Fig. 1a). TDX_{ON} is obtained by completely reducing TDX. As TDX might also turn on due to background hydrolysis of the carbonate linker, we made TDX_{OFF} in which fluorescein is caged by a non-reducible benzyloxycarbonate moiety (Fig. 1a–1b, SI scheme 2). Thus, TDX_{OFF} reports non-specific hydrolysis and reveals the specificity of disulfide exchange reported by TDX. The synthesis and characterization of TDX, TDX_{ON} and TDX_{OFF} are described in the supplementary information (SI Scheme 1–2 & SI Fig. 1a).

In the presence of glutathione (GSH, 5 mM) at pH 7.2, TDX fluorescence at 520 nm (G, fluorescein) increases with time, while the fluorescence of the normalizing module, at 590 nm (R, rhodamine), remains constant (Fig. 1c). Fig. 1d shows the G/R ratio of emission intensities as a function of time, which reveals that the reaction is 80% complete in 30 min. Importantly, under comparable conditions, TDX_{OFF} showed no increase in G/R ratio, indicating that the fluorescence increase observed in TDX is due to disulfide exchange (Fig. 1d, SI Fig. 1b).

TDX detects disulfide exchange in late endosome in vivo

Although genetically encoded redox reporters can be applied to study redox in the cytosol[18,25] they cannot be used in organelles due to the acidic lumenal pH in organelles. Particularly in *Caenorhabditis elegans,* the glutathione redox potential varies in different tissues and cell types, yet there is no information available at the sub-cellular level[26]. We therefore sought to deploy the TDX reporter system to map intra-endosomal thiol disulfide exchange along the endolysosomal pathway in *C. elegans.*

DNA nanodevices selectively label coelomocytes in *C. elegans* by targeting scavenger receptor-mediated endocytosis[24] Upon injection of 2 μM TDX into the pseudocoelom of wild type (N2) nematodes, fluorescence images of live worms were acquired in G and R channels as a function of time. For each time point we constructed ratiometric maps of G/R

intensities represented in pseudocolour (Methods, Fig. 2a). We observed that the G/R ratio was maximal at 20 minutes post injection and remained almost constant thereafter (Fig. 2a–b). A similar experiment using TDX_{OFF}, gave a G/R ratio that remained unchanged (Fig. 2b, SI Fig. 2). This indicates that the increase in G/R ratio shown by TDX is due to thiol-disulfide exchange and not from esterolysis.

The tripartite reporter comprising TDX_{ON}, TDX_{OFF} and TDX, jointly corrects for any pH effects on the fluorescence of the sensor module. For example the lumenal pH decreases along the endocytic pathway which could affect the fluorescein intensity. We correct for this by performing three sets of experiments at each timepoint, injecting either TDX_{ON}, TDX_{OFF} or TDX, obtaining G and R images, heat maps and G/R values (Fig. 2b). We calculate the percentage response of TDX (Fig. 2c) as a function of time using the equation 1 (Methods section). This yielded a sigmoidal curve for thiol-disulfide exchange as a function of time where, 20 min post injection the reaction was complete (Fig. 2c).

For the first 10 minutes, TDX response is negligible, and then starts reacting at t = 15 min and by t = 20 minutes, the reaction is ~ 80% complete. Colocalization studies with endosomal markers in transgenic nematodes were performed. Rhodamine labelled dsDNA, denoted TDX^R was injected in nematodes expressing GFP::RAB-5 as an early endosomal marker, GFP::RAB-7 as an late endosomal/lysosomal marker and LMP-1::GFP as a lysosomal marker (Fig. 2d). At t = 20 min post injection TDX^R showed 85% colocalization with GFP::RAB-7 (Fig. 2e) indicating its localization in the late endosome. This reveals that thiol-disulfide exchange of TDX occurs in late endosomes in coelomocytes.

The observed intra-endosomal disulfide exchange could be mediated by small molecules like cysteine, glutathione, H2S etc., or by enzymes[16,27]. Using a well-characterized, icosahedral DNA nanocapsule reporter system (SI Fig. 3 & 4)[28,29], we found that uncatalyzed thiol-disulfide exchange mediated by small biologically available thiols was negligible.

PDI-3 and TRX-1 catalyse thiol exchange in late endosomes

Next, we sought to identify the protein players, if any, that mediated intra-endosomal disulfide reduction in coelomocytes. Proteins that catalyse disulfide exchange generally contain thioredoxin domains e.g., thioredoxins or protein disulfide isomerases[30]. Using BLASTP[31] we found ~23 proteins in the *C. elegans* genome that contained at least one thioredoxin domain (SI Fig. 16). We excluded seven that contained either a mitochondrial or nuclear localization sequence, which precluded their endosomal localization (SI Table 2). We then knocked down each of the fifteen candidate genes by RNA interference (RNAi) and, in each genetic background, we quantitated the percentage response of the TDX reporter due to intra-endosomal thiol disulfide exchange (Fig. 3b). We obtained two clear hits, where knocking down *pdi-3* or *trx-1* showed 50% and 40% reduction in disulfide exchange respectively as compared to wild type nematodes (Fig. 3b). Simultaneous knockdown of both *pdi-3* and *trx-1* in nematodes showed a dramatic reduction of disulfide exchange, nearly comparable to G/R values seen with TDX_{OFF} (Fig. 3a). This indicates that disulfide reduction in the late endosome is predominantly due to *pdi-3* and *trx-1.* The

efficiency of RNAi knockdown of relevant genes were confirmed by RT-PCR followed by gel electrophoresis (Fig. 3c).

TRX-1 mainly reduces several disulfide containing proteins, and thereby serves to enhance the activity of stronger reducing proteins e.g., protein disulfide isomerases (PDIs). In fact, the oxidation potential of PDIs are nearly 50 fold higher than thioredoxin[32], suggesting that PDI-3 could also function along with TRX-1 at the acidic pH in the late endosome[24]. Thioredoxin-1 (TRX-1) is maximally present in the cytosol, while PDI-3 is maximally present in the endoplasmic reticulum (ER) due to its strong ER retention signal[33]. It is notable that despite the presence of PDI-3 and TRX-1 on the plasma membrane, as well as 1–10 μM extracellular glutathione[34], our nanodevice reporters are reduced specifically in the late endosome. This reveals the existence of a minor, catalytically active pool of PDI-3 and TRX-1 in the late endosome where they bring about intra-endosomal disulfide exchange.

Endosomal disulfide exchange facilitates pathogen infection

Disulfide exchange is co-opted by pathogens like *B. cenocapacia, C. diphtheriae,* the HIV virus, the rotavirus ECwt, ganjam virus etc. so that they can efficiently infect host cells[35–39]. We addressed significance of the catalytic activities of our hits PDI-3 and TRX-1 in endosomes, by investigating their roles in mediating pathogen infection. For this, we used a previously established *Corynebacterium diphtheriae* infection model in *C. elegans*[39]. Briefly, *C. diphtheriae* secretes an AB toxin called diphtheria toxin (DT), comprising a non-toxic B-subunit (DT-B) and a toxic A-subunit (DT-A) linked through a disulfide bond. This disulfide bond is reduced within the endosomes and DT-A thereby translocates into the cytosol, inhibiting protein synthesis in the host cell. Disulfide reduction is thus a critical step to bring about toxin infection (SI. Fig. 8).

We used the transgenic nematode *cl2070,* which expresses GFP under a heat shock promoter *hsp-16.2* in all tissues. Successful infection by *C. diphtheria* is expected to result in cytosolic DT-A compromising protein synthesis leading to nematodes that fail to express GFP in the pharynx upon heat-shock[40]. Accordingly, nematodes infected with *C. diphtheriae* showed significantly less GFP in the pharynx compared to non-infected nematodes (Fig. 4a). Notably, GFP intensity in the gut were comparable in both infected and non-infected nematodes as the site of action of *C. diphtheriae* is not the gut, but the pharynx (Fig. 4b–4c and SI Fig. 6–7)[39].

Next, we examined the consequences of inhibiting intra-endosomal disulfide reduction on DT infection, by knocking down *pdi-3* and/or *trx-1* in this infection model. We observed that *trx-1*, but not *pdi-3,* knockdowns show retention of pharyngeal GFP expression upon treatment with *C. diphtheriae* (Fig. 4a–4b). This indicates that by knocking down endosomal disulfide exchange brought about by the minor endosomal population of thioredoxin-1 impedes DT infection by reducing the extent of cytosolic translocation of the DT-A. Knocking down both *pdi-3* and *trx-1* also prevents DT infection (Fig. 4b). In coelomocytes, we observe that PDI-3 *and* TRX-1 both are involved in endosomal disulfide reduction but in the case of DT infection only TRX-1 is responsible. Even though both TRX-1 and PDI-3 were responsible for intra-endosomal disulfide reduction, we found that DT infection

depends on the minor pool of TRX-1, and not PDI-3. This is also consistent with *in vitro* studies that show that the intra-chain disulfide bond of DT is a good substrate for thioredoxin-1 at acidic pH[41]. Our findings imply that DT preferentially exploits intra-endosomal reduction by thioredoxin-1 *in vivo* and that inhibiting this minor pool could be a promising route to impede DT infection.

TRX-1 mediates endosomal disulfide exchange in human cells

Next, we sought to generalize this reporter technology by probing disulfide reduction in a mammalian cell culture system. All TDX reporters undergo scavenger receptor mediated endocytosis in HeLa cells upon incubation with 1 μM of any TDX reporter[42]. We could therefore follow disulfide reduction as a function of time using TDX reporters as described (SI Fig.11). While we observed no disulfide reduction for the first 2 h, TDX reporters started responding at t = 3 h and the reaction was complete by t = 4 h (Fig. 5a–5b). The analogous experiment with TDX_{OFF} showed negligible change in G/R ratio (Fig. 5a). We pharmacologically inhibited disulfide isomerases in HeLa cells using N-ethyl maleimide (NEM) or by blocking surface and endosomal thiols using 5,5'-dithio-bis-(2-nitrobenzoic acid) (DTNB). Both treatments reduced reporter response by ~90% confirming that endosomal disulfide reduction was indeed responsible for the signal increase (Fig. 5d & SI Fig. 12).

Colocalization studies with various endosomal markers indicated that the observed disulfide reduction occurred in the late endosome. We pulsed HeLa cells expressing Rab5-RFP as an early endosomal marker or Rab7-RFP as a late endosomal marker TDX bearing a single Alexa-647 fluorophore (TDX^{A647}) and assayed for colocalization after a 3 h chase. We observed ~70% colocalization with Rab7-RFP and insignificant colocalization with Rab5-GFP. Lysosomes were labeled with TMR-dextran through fluid phase endocytosis after a 1 h pulse and 12 h chase. HeLa cells pre-labelled thus were then pulsed and chased with TDX^{A647} as above showed negligible colocalization with lysosomes (Fig. 5c).

To identify the major protein player involved in this reduction, we knocked down the human analogues of PDI-3 and TRX-1 by RNAi. HeLa cells where Erp57 and TRX-1 were each knocked down were investigated using the tripartite reporter system and the G/R ratios were obtained. We observed that disulfide reduction in TRX-1 depleted cells was reduced by >70% compared to normal cells, while Erp57 depleted cells showed negligible change (Fig. 5d, SI Fig. 12). This indicates that in mammalian cells, a minor pool of endosomal resident TRX-1 plays a major role in endosomal disulfide reduction.

Summary

The modular design of our DNA-based tripartite fluorescent reporter system enables quantitative imaging of intra-endosomal disulfide exchange *in situ* in coelomocytes of *C. elegans* as well as in mammalian cells. It revealed that thiol-disulfide exchange along the endolysosomal pathway occurs mainly in the late endosome. We ruled out small molecule thiol-mediated reduction in late endosomes, implicating the action of proteins in these acidic compartments. In fact, the pK_a of the N-terminal active site cysteine of PDI can be as low as

4.8, while that of thioredoxins can range between ~6.0–7.0[43]. This is in consistent with the rapid thiol reduction kinetics we observe in the acidic late endosome lumen, supporting that disulfide exchange is likely to be enzyme catalyzed.

Quantitative imaging of thiol-disulfide exchange in RNAi knockdowns of various candidate genes revealed that PDI-3 and TRX-1 were the enzymes responsible for the observed intra-endosomal disulfide reduction *in vivo*. Though PDI-3 and TRX-1 are predominantly localized in the endoplasmic reticulum (ER) and cytosol respectively[33,44] a minor pool of these proteins is localized in sub-cellular compartments where they perform critical functions. Using a diphtheria toxin infection model, we showed that inhibiting the catalytic activity of this minor population of enzyme inside the endosome protects the host cell from pathogen infection. The reporter system revealed that TRX-1 was also responsible for disulfide reduction in late endosomes of human cells. Given the large number of toxins and pathogens that exploit intra-endosomal disulfide reduction to bring about infection[38], our work suggests that the selective inhibition of intra-endosomal disulfide exchange could be of interest to develop anti-infectives.

The advantage of this tripartite reporter system is the newfound ability to directly and selectively assay, in live cells and with spatial information, the enzyme activity of protein populations in organelles by localizing the detection chemistry within the organelle (SI Figure 14–15). The stoichiometric precision of DNA hybridization enables two major advantages, unique to DNA-based probes and inaccessible to any other reporter technology: (i) molecularly identical probes, with fixed, uniform sensor to normalizer ratios that quantify a given analyte with accuracies unmatched by any other molecular scaffold. (ii) “Plug-and-play” capability due to its modular nature: Once a DNA-probe is validated, it can be directly used in a host of other organelle locations by simply swapping out one organelle targeting module for any other.

It can thus be readily integrated with existing diversity of small molecule reporters and enzyme-cleavage chemistries to provide robust readouts exclusively in organelles *in situ* within living cells (SI table 3). For example, lysosomal enzyme chemistries may be integrated to measure lysosomal enzyme activity *in situ* with several applications in lysosomal storage disorders[45]. Catalytic activity of endosomal proteases such as cathepsin B, cathepsin D, or β-secretase-1 results in protein processing events leading to cancer and Alzheimer’s disease[46,47]. Protease action by proprotein convertases in the Golgi underlie neurogenesis, TGF-β signalling and AB_5 toxin infection[48]. The ability of DNA nanodevices to selectively quantitate sub-cellular enzymatic cleavage in live cells could provide new diagnostics and drug discovery assays.

It can be also be integrated with newer reporting strategies that probe enzymatic function such as activity based protein probes to identify enzymatic activity in cellular compartments[49]. The advent of transformative technologies such as fluorescent proteins, the SNAP-tag[50] or the Halo-tag[57] ushered in a new era of visualizing proteins[56] *in situ* by enabling methods to image the major population of any protein of interest. The organelle-targetable nanodevice system described here effectively complements these powerful

technologies by selectively interrogating minor populations of enzymes involved critical cellular functions, which cannot otherwise be studied.

Methods

Materials and Methods.

All the chemicals used for the synthesis were purchased from commercial source (Sigma, USA). ^{1}H NMR and ^{13}C NMR spectra of the newly synthesized compounds were recorded on a Bruker AVANCE II+, 500MHz NMR spectrophotometer. TMS is used as an internal standard. Mass spectra were recorded in Agilent 6224 Accurate-Mass TOF LC/MS. HPLC purified oligonucleotides conjugated with either fluorophore or azide functional group were obtained from Integrated DNA Technologies (IDT, USA). All oligonucleotides are ethanol precipitated and quantified by UV absorbance at λ= 260 nm.

Synthesis of TDX reporter.

Rhodamine and azide labelled DNA-strand (O-Rhodamine Red X and O-azide) (Table-1) were mixed in equimolar concentration (25 μM each) in 20 mM phosphate buffer containing 100 mM KCl at pH 7. The mixture was heated at 90°C for 10 min and then cooled down to room temperature at the rate of 5°C/15 min and stored in 4°C for overnight to form a complete DNA-duplex.

Next, Rhodamine DNA-duplex was conjugated with compound **8** by reported copper catalysed azide-alkyne click chemistry protocol[51]. Initially 20 μL rhodamine conjugated DNA duplex was (25 μM) diluted in 13.5 μL water, to that of 3 μL compound **8** (5 mM) in DMSO was added. Then 1:1 (v/v) premix solution of 7.5 μL of $CuSO_4$ (0.1 M) and THPTA (0.2 M) was added to it. The reaction mixture was degassed with N_2 for 2 min and followed by this 6 μL of sodium ascorbate (0.1 M) was added. The mixture was further degassed for 0.5 min and then stirred at room temperature for 1 h under N_2 atmosphere. Native PAGE (20 wt%) showed complete formation of TDX reporter (Fig. 1a and Supplementary Fig. 1a). Subsequently, the reaction mixture was diluted with pH = 6.0 phosphate buffer and washed with 10% acetonitrile (to remove excess of compound **8** using Amicon Ultra-0.5mL centrifugal filter (MWCO 3 kDa). The same washing procedure was continued until the filtrate showed no trace of compound **8** using fluorescence spectroscopy (λ_{em} = 520 nm). Followed by, we performed native gel electrophoresis and monitored by fluorescence which reveals negligible single strand in our preparations.

Synthesis of TDX_{ON} reporter.

10 μL TDX reporter (8 μM) was mixed with 1 μL (5 mM) NaSH solution in 0.1 M phosphate buffer at pH 7.4 and stirred for 2 h at room temperature. Followed by this, excess thiol was removed by ultracentrifugation using Amicon filter (MWCO 3 kDa) to obtain TDX_{ON} reporter (see Fig. 1a).

Synthesis of TDX_{OFF} reporter.

TDX_{OFF} reporter was prepared in a similar procedure like TDX reporter, except compound **9** was used here instead of compound **8**. The formation of TDX_{OFF} reporter was characterized by using gel electrophoresis (see Supplementary Fig. 1a).

Conjugation of compound 8 with azido dextran.

2 mg Azido functionalized dextran (10 kDa, 2–3 azido group per dextran) was dissolved in 90 μL milli Q water. 20 μL of compound **8** (5mM), followed by 50 μL $CuSO_4$ (0.1 M) and THPTA (0.2 M) mixture (1:1) was added to it. The reaction mixture was degassed for 2 min and 40 μL sodium ascorbate (0.1 M) was added, purged again with N_2 for 0.5 min before stirring at room temperature for 1 h under N_2 atmosphere. The resulting dextran conjugate was diluted with milli Q water and washed with the 10% acetonitrile to remove excess of compound **8** using an Amicon filter (MWCO 3 kDa).

Self-assembly of $I^{A647}{}_{FD}$.

Half icosahedrons (VU_5 and VL_5) was prepared as describe in literature[52]. In order to synthesize the DNA-icosahedron, VU_5 and VL_5 (3 μM each, 30 μL, in 50 mM phosphate buffer, pH 6.0) containing 2 mM solution of the compound **8** conjugated dextran (FD) (M. Wt.~10 kDa) was mixed in an eppendorf tube and heated to 37 °C for 30 min. The temperature was brought down to 20 °C with a rate of 1 °C/ 3 min and followed by incubation for 2 h. The reaction mixture was transferred to refrigerator at 4°C for further incubation for longer time periods up to 48 h. The formation of $I^{A647}{}_{FD}$ was characterized by 0.8 wt% Agarose gel electrophoresis (Supplementary Fig. 3a).

Preparation of $I^{A647}{}_{FD\text{-}ON}$.

10 μL solution (3 μM) of $I^{A647}{}_{FD}$ was treated with 1 μL (5 mM) NaSH solution in 0.1 M phosphate buffer at pH 7.4 and stirred for 2 h at room temperature. The excess thiol was removed by ultracentrifugation using Amicon filter (MWCO 3 kDa).

Determination of size of different thiol.

DLS experiment was done in Wyatt Dynapro Nanostar & Plate Reader. Samples were dissolved in milli-Q water or buffer filtered through 0.22 μm filter to remove dust particles. Samples were illuminated with laser wavelength of 658 nm, at a sensitivity of 80% and a scattering angle set at 90° with a 10 second acquisition time for data collection. Percentage intensity observed for each sample, was plotted against respective R_h values. The size of PEG-SH (3.2 kDa), Dex-SH (10 kDa) and Dex-SH (40 kDa) was determined from DLS measurements. Aqueous solution of the free thiol containing polymer (1 mg/mL) was again filtered in a dust-free environment, and DLS measurement was carried out with this solution. For glutathione, cysteine and H_2S, we used Chem 3D ultra 8.0 software and used the end to end distance of the energy minimized structure as diameter of those molecules.

In vitro fluorescence measurements.

Fluorescence spectra were recorded on a FluoroMax-4 instrument (Horiba Jobin Yvon). TDX and TDX_{OFF} reporter was diluted to 100 nM in 0.1 M phosphate buffer at pH = 7.2 in

presence or absence of 5 mM GSH. These samples were excited at 450 nm (for fluorescein emission) and 575 nm (for rhodamine emission). The emission spectrum was collected between 460–600 nm and 590–700 nm for fluorescein and rhodamine respectively at different time point. Three independent measurements were recorded for each sample (Fig. 1c). We checked the specificity of reporter dye towards thiol disulfide exchange reaction; we treated the reporter dye (compound **8**) with different metal ions and amino acids. We have observed no reaction with any of the metal ions and amino acids tested except cysteine (Supplementary Fig. 1c).

In order to check the substrate availability for disulfide exchange reaction with $I^{A647}{}_{FD}$ as a function of the size of reactive thiols (1 mM), we have treated $I^{A647}{}_{FD}$ (3 μM) and FD with various thiol and checked the emission spectra after 1 h of incubation. For monitoring the emission spectra, the samples were excited at 450 nm (fluorescein channel) and 647 nm (Atto 647N channel). The emission spectrum was collected between 460–600 nm and 650–750 nm for fluorescein and Atto 647N respectively. (Supplementary Fig. 3b).

Protocols for *C. elegans* and strains.

Standard methods for the maintenance of *C. elegans* were followed. We used wild type *C. elegans* strain isolated from Bristol (Strain N2). Mutant strain used for the experiment is *VC586 [pdi-1(gk271) III].*

Transgenic strains used for this study are;

- **i.** *cdIs131 [pcc1::GFP::rab-5 + unc-119(+) + myo-2p::GFP],* a transgenic strain that express GFP-fused early endosomal marker RAB-5 inside coelomocytes.
- **ii.** *cdIs66 [pcc1::GFP::rab-7 + unc-119(+) + myo-2p::GFP],* a transgenic strain that express GFP-fused late endosomal / lysosomal marker RAB-7 inside coelomocytes.
- **iii.** *pwIs50 [lmp-1::GFP + Cbr-unc-119(+)],* a transgenic strain that express GFP-fused lysosomal marker LMP-1.
- **iv.** *dvIs70 [hsp-16.2p::GFP + rol-6(su1006)],* a transgenic strain which have GFP expression under heat shock protein HSP-16.2 promoter. It express GFP in presence of mild heat shock.

Protocols for *C. diphtheria* strains and growth conditions.

Two different kind of *C. diphtheria* strain have been used for pathogen infection to *C. elegans.* They are toxic *C. diphtheria* (ATCC 13812) which produces diphtheria toxin (DT) and less toxic C. diphtheria (ATCC 39526) (DTΔ149) which produces mutated diphtheria toxin. For toxic and less toxic *C. diphtheria,* we have used tryptic soy broth with 5 % sheep blood and ATCC medium: 1417 Low Iron YC medium as a culture medium respectively and inoculate for 24 h at 37°C as described in ATCC website.

TDX and I^{A647}_{FD} reporters targeted to coelomocyte of *C. elegans.*

For coelomocyte targeting[52], we microinjected 2 μM of TDX reporter in the dorsal side in the pseudocoelom, just opposite to the vulva, of 1-day-old wild type hermaphrodites. Injected worms then placed in a new NGM agar containing petriplate at 22°C for incubation at different time point. Followed by this they were mounted in an Agar pad (2.0%) and anaesthetized using 40 mM sodium azide in M9 buffer and performed fluorescence imaging experiment. Same protocol was followed in the case of TDX_{OFF} and TDX_{ON}.

DNA-icosahedron encapsulated reporters, (I^{A647}_{FD}, $I^{A647}_{FD\text{-}ON}$ and $I^{A647}_{FD\text{-}OFF}$, 3 μM each) were injected to the wild type worms as described earlier and imaged at 30 min post-injection period.

Colocalization of TDX^R with late endosomes in coelomocytes.

In order to investigate the localization of TDX reporter at 20 min post injection, we have conducted co-localization experiment using *cdIs131, cdIs66* and *pwIs50* transgenic worms. For this, we have injected 2 μM rhodamine DNA-duplex to these worms and imaged after 20 min. We have observed ~ 85% co-localization of TDX reporter with RAB-7::GFP positive vesicles, which marks late endosomal and lysosomal compartments (see Fig. 2d and Supplementary Fig. 8).

RNAi experiment.

We used BLASTP[53] to look for thioredoxin domain containing protein in *C. elegans* genome. Bacteria of our interest, expressing double-stranded RNA (see Supplementary table 2) were obtained from Ahringer RNAi library[54] and Vidal Unique[55]. Cloned bacteria were fed to the worms and ~ 60 one-day adults of the F1 progeny were used for screening. The Ahringer or Vidal unique library did not contain bacterial clones for *Y73B6BL.2* and hence this gene was not included in this screen.

We assayed mRNA levels of the candidate genes by RT – PCR. Briefly, we isolated total RNA using the Trizol-chloroform method; 2.5 μg of total RNA was converted to cDNA using oligo-dT primers. 5 μl of the reverse transcription reaction was used to set up a PCR using gene-specific primers. PCR products were analysed on a 1.5 % agarose-TAE gel (see Fig. 3c). Size of the PCR products expected for each gene were: actin (360 bp), *pdi-3* (682 bp), *C30H7.2* (798 bp), *trx-2* (316 bp), *trx-1* (261 bp).

hsp-16.2::GFP experiments to measure DT infection-triggered translational inhibition.

hsp2::GFP experiments were modified from literature reported procedure[56]. Briefly the fresh culture of either toxic or less toxic *C. diphtheria* (DTA149) were seeded into the nematode growth medium (NGM) containing agar plate. Each plates contains 50 μL of bacterial culture. After that the plates were kept at 25°C for 24 h for drying the liquid medium on agar. WT or different genetic background worms were washed onto *C. diphtheria* seeded plates and incubated for 6 h for infection at 25°C followed by washed and transferred to a plat containing 0P50 or the bacteria carrying the RNAi clone in it. These *C. elegans* then subjected to 1 h heat shock at 37°C and then returned to 25°C for another 1 h. After that the worms are imaged for GFP expression. GFP expression was quantified by keeping the

microscope settings fixed for all samples. The standard region of pharynx and intestine was chosen for GFP intensity measurement (see Supplementary Fig. 6). For the intestine we chose a region towards the posterior of intestine because it showed the robust GFP expression. The GFP intensity was measured for at least 20 worms in each genetic background worm.

Cell culture.

HeLa cells were a kind gift from Prof. Chuan He (Department of Chemistry, the University of Chicago). Mouse macrophages J774A.1cells were a kind gift from Prof Deborah Nelson, (Department of Pharmacological and Physiological Sciences, the University of Chicago). These cells were cultured in DMEM-F12 with 10% FBS, 100 U/mL penicillin, 100 μg/ mL of streptomycin and maintained at 37 ^{o}C under 5% CO2. Bone marrow derived macrophages (BMDMs) were isolated from femurs and tibia of male C57BL/6 mice and were obtained from Prof. Lev Becker lab (Ben May Department for Cancer Research, University of Chicago). Cells were differentiated to macrophages using murine M-CSF for 6 days. For LPS activation, cells were treated with 20 ng/mL LPS for 24 h. All animal studies are in compliances with ethical regulations approved by the University of Chicago Institutional Animal Care and Use Committee (ACUP 72209).

Microscopy and ratiometric image analysis.

Wide-field microscopy was performed on an IX83 inverted microscope (Olympus Corporation of the Americas, Center Valley, PA, USA) using a 60X, 1.42 NA, phase contrast oil immersion objective (PLAPON, Olympus Corporation of the Americas, Center Valley, PA, USA) and Evolve® Delta 512 EMCCD camera (Photometrics, USA). Filter wheel, shutter and CCD camera were controlled using Metamorph Premier Version 7.8.12.0 (Molecular Devices, LLC, USA), appropriate for the fluorophore used. Images on the same day were acquired under the same acquisition settings. Confocal imaging was carried out on a Leica SP5 II STED-CW super-resolution microscope, using an Argon ion laser for 488 nm excitation and DPSS for 561 nm excitation with a set of dichroic, excitation, and emission filters suitable for each fluorophore. Crosstalk and bleed-through were measured and found to be negligible between GFP / fluorescein and Rhodamine.

All the images were background subtracted by using mean intensity calculated from an adjacent cell-free area. Fluorescein and Rhodamine images were colocalized and endosomes showing good colocalization were analysed using ImageJ-Win64 software (NIH). Mean fluorescence intensity in each endosome was measured in fluorescein (G) and rhodamine (R) channels. A ratio of G/R intensities was calculated from these values. Pseudocolour images were generated by measuring the G/R ratio per pixel. Using ImageJ software, pixels were then colour coded accordingly to indicate differences between high and low G/R ratios.

% Response Calculation.

Percentage response of the TDX reporter at different time points for the wild type worm and for the RNAi worm (20 min) were calculated using the following equation (1).

$$\%\text{Response}=\left[\left({}^{G/R}\text{TDX}-{}^{G/R}\text{TDX}_{OFF}\right)/\left({}^{G/R}\text{TDX}_{ON}-{}^{G/R}\text{TDX}_{OFF}\right)\right]\times 100 \quad (1)$$

(Here, ${}^{G/R}\text{TDX}$, ${}^{G/R}\text{TDX}_{OFF}$ and ${}^{G/R}\text{TDX}_{ON}$ indicate the observed fluorescence intensity ratio of fluorescein to that of rhodamine at a given time point by using TDX, TDX_{ON} and TDX_{OFF} reporters respectively).

Targeting TDX reporter to endolysosomal pathway in HeLa cells.

We incubated HeLa cells with TDX reporter (1 μM) containing DMEM without FBS for 1 h at 37 °C. Cells were then washed with PBS (pH=7.4) thrice to remove any un-internalized TDX nanodevice and incubated for various chase times in DMEM complete media. Prior to imaging, cells were washed with PBS and imaged in HBSS (Hank's Balanced Salt Solution, GE healthcare) buffer. Similar protocol was followed for TDX_{ON} and TDX_{OFF} reporters.

RNAi knockdown and pharmacological inhibition in HeLa cells.

All relevant siRNAs were procured from Dharmacon, Inc. HeLa cells were split on imaging dish at 1×10^4 seeding density. After 16 h in culture, the cells were transfected with siRNAs using DharmaFECT1 (Dharmacon; Catalogue No: T-2001–01) transfection reagent according to the manufacturer's protocol. For Erp57 and TRX-1 knockdown, HeLa cells were transfected with Erp57 siRNA[57] (5'-GGGCAAGGACUUACUUAUUTT-3 ') and TRX-1 siRNA (Dharmacon, Inc., Catalogue No: M-006340–010005). As a negative control, we used the NC siRNA (Dharmacon, Inc., Catalogue No: D-001210–01-05). After 72 h of transfection, cells were incubated with the tripartite TDX reporter for 1 h in DMEM without FBS and chased for 3 h in complete media and imaged as described earlier.

For pharmacological inhibition, cells were incubated with complete media containing either NEM (10 μM) or DTNB (100 μM) for 1 h, followed by 1 h of incubation with TDX reporter in DMEM without FBS. The cells were chased for 4 h in complete media containing either 10 μM NEM or 100 μM DTNB, washed with PBS and imaged as described in HBSS buffer containing either 10 μM NEM or 100 μM DTNB so that the relevant pharmacological inhibitor was always present.

Cathepsin C activity assay.

J774A.1 cells with or without Cathepsin inhibitor E64 were pulsed with 500 nM of either **Cat** or $\textbf{Cat}_{\textbf{ON}}$ probes (SI Figs. 14 & 15) separately for 30 min at 37° C. After 1 h, cells were washed and imaged in the Rhodamine (G, λ_{em} = 520 nm) and Alexa 647 (R, λ_{em} = 670 nm) channels. The $\textbf{Cat}_{\textbf{ON}}$ probe provides the maximum possible ratiometric signal (G/R) if the **Cat** probe was completely cleaved. All G/R values were normalized to that of $\textbf{Cat}_{\textbf{ON}}$. Similar pulse and chase experiments were performed in BMDMs with 200 nM **Cat** probes. BMDMs were then subjected to flow cytometry on a FACSCanto™ II flow cytometer (SI Fig.15).

Statistical Analysis.

We used Graphpad unpaired t-test calculator for all statistical significance calculations (https://www.graphpad.com/quickcalcs/ttest1/).

Supplementary Material

Refer to Web version on PubMed Central for supplementary material.

Acknowledgments

We thank Jon Clardy, John Kuriyan, Souvik Modi and Ai Lin Chun for valuable comments on this work. We thank the Integrated Light Microscopy facility at the University of Chicago, the Caenorhabditis Genetic Center (CGC), Johnny Fares and Mark Edgley for *C. elegans* strains, Michael Glotzer and Frederick M. Ausubel for RNAi clones and valuable discussions, Sean Crosson for BSL facility for *C. diphtheriae* work, Chang Cui for bone marrow derived macrophages and flow cytometry. This work was supported by the University of Chicago Women's Board, Chicago Biomedical Consortium with support from the Searle Funds at The Chicago Community Trust, C-084 as well as a CBC post-doctoral research grant (PDR-073) and University of Chicago start-up funds to Y.K. Y.K. is a Brain Research Foundation Fellow.

References

1. Huang S-H, Li Y, Zhang J, Rong J & Ye S Epidermal growth factor receptor-containing exosomes induce tumor-specific regulatory T cells. Cancer Invest 31, 330–335 (2013). [PubMed: 23614656]
2. Efeyan A, Comb WC & Sabatini DM Nutrient-sensing mechanisms and pathways. Nature 517, 302–310 (2015). [PubMed: 25592535]
3. Dean N & Pelham HR Recycling of proteins from the Golgi compartment to the ER in yeast. J. Cell Biol. 111, 369–377 (1990). [PubMed: 2199456]
4. Bhuniya S et al. An activatable theranostic for targeted cancer therapy and imaging. Angew. Chem. Int. Ed. Engl. 53, 4469–4474 (2014). [PubMed: 24644015]
5. Lee MH et al. Hepatocyte-targeting single galactose-appended naphthalimide: a tool for intracellular thiol imaging in vivo. J. Am. Chem. Soc. 134, 1316–1322 (2012). [PubMed: 22171762]
6. Crivat G & Taraska JW Imaging proteins inside cells with fluorescent tags. Trends Biotechnol. 30, 8–16 (2012). [PubMed: 21924508]
7. Los GV et al. HaloTag: a novel protein labeling technology for cell imaging and protein analysis. ACS Chem. Biol. 3, 373–382 (2008). [PubMed: 18533659]
8. Gething MJ & Sambrook J Protein folding in the cell. Nature 355, 33–45 (1992). [PubMed: 1731198]
9. Mesecke N et al. A disulfide relay system in the intermembrane space of mitochondria that mediates protein import. Cell 121, 1059–1069 (2005). [PubMed: 15989955]
10. Burgoyne JR et al. Cysteine redox sensor in PKGIa enables oxidant-induced activation. Science (80-.). 317, 1393–1397 (2007). [PubMed: 17717153]
11. Wang M-Y et al. A redox switch in C-reactive protein modulates activation of endothelial cells. FASEB J. 25, 3186–3196 (2011). [PubMed: 21670067]
12. Collins DS, Unanue ER & Harding CV Reduction of disulfide bonds within lysosomes is a key step in antigen processing. J. Immunol. 147, 4054–4059 (1991). [PubMed: 1721638]
13. Guermonprez P et al. ER-phagosome fusion defines an MHC class I cross-presentation compartment in dendritic cells. Nature 425, 397–402 (2003). [PubMed: 14508489]
14. Stolf BS et al. Protein disulfide isomerase and host-pathogen interaction. ScientificWorldJournal 11, 1749–1761 (2011). [PubMed: 22125433]
15. Maiti S et al. Gemcitabine-coumarin-biotin conjugates: a target specific theranostic anticancer prodrug. J. Am. Chem. Soc. 135, 4567–4572 (2013). [PubMed: 23461361]
16. FeenerS E, Shene W-C & Ryser H Cleavage of Disulfide Bonds in Endocytosed Macromolecules.
17. Shen WC, Ryser HJ & LaManna L Disulfide spacer between methotrexate and poly(D-lysine). A probe for exploring the reductive process in endocytosis. J. Biol. Chem. 260, 10905–10908 (1985). [PubMed: 4030773]
18. Meyer AJ & Dick TP Fluorescent protein-based redox probes. Antioxid. Redox Signal. 13, 621–650 (2010). [PubMed: 20088706]

19. Chakraborty K, Veetil AT, Jaffrey SR & Krishnan Y Nucleic Acid-Based Nanodevices in Biological Imaging. Annu. Rev. Biochem. 85, 349–373 (2016). [PubMed: 27294440]
20. Liu J, Cao Z & Lu Y Functional nucleic acid sensors. Chem. Rev. 109, 1948–1998 (2009). [PubMed: 19301873]
21. Famulok M, Hartig JS & Mayer G Functional aptamers and aptazymes in biotechnology, diagnostics, and therapy. Chem. Rev. 107, 3715–3743 (2007). [PubMed: 17715981]
22. Modi S, Nizak C, Surana S, Halder S & Krishnan Y Two DNA nanomachines map pH changes along intersecting endocytic pathways inside the same cell. Nat. Nanotechnol. 8, 459–467 (2013). [PubMed: 23708428]
23. Saha S, Prakash V, Halder S, Chakraborty K & Krishnan Y A pH-independent DNA nanodevice for quantifying chloride transport in organelles of living cells. Nat. Nanotechnol. 10, 645–651 (2015). [PubMed: 26098226]
24. Surana S, Bhat JM, Koushika SP & Krishnan Y An autonomous DNA nanomachine maps spatiotemporal pH changes in a multicellular living organism. Nat Commun 2, 340 (2011). [PubMed: 21654640]
25. Gutscher M et al. Real-time imaging of the intracellular glutathione redox potential. Nat. Methods 5, 553–559 (2008). [PubMed: 18469822]
26. Romero-Aristizabal C, Marks DS, Fontana W & Apfeld J Regulated spatial organization and sensitivity of cytosolic protein oxidation in Caenorhabditis elegans. Nat Commun 5, 5020 (2014). [PubMed: 25262602]
27. Yang J, Chen H, Vlahov IR, Cheng J-X & Low PS Evaluation of disulfide reduction during receptor-mediated endocytosis by using FRET imaging. Proc. Natl. Acad. Sci. USA 103, 13872–13877 (2006).
28. Bhatia D et al. Icosahedral DNA nanocapsules by modular assembly. Angew. Chem. Int. Ed. Engl. 48, 4134–4137 (2009). [PubMed: 19222079]
29. Veetil AT, Jani MS & Krishnan Y Chemical control over membrane-initiated steroid signaling with a DNA nanocapsule. Proc. Natl. Acad. Sci. USA 115, 9432–9437 (2018). [PubMed: 29531078]
30. Sevier CS & Kaiser CA Formation and transfer of disulphide bonds in living cells. Nat. Rev. Mol. Cell Biol. 3, 836–847 (2002). [PubMed: 12415301]
31. Altschul SF, Gish W, Miller W, Myers EW & Lipman DJ Basic local alignment search tool. J. Mol. Biol. 215, 403–410 (1990). [PubMed: 2231712]
32. Hawkins HC, Blackburn EC & Freedman RB Comparison of the activities of protein disulphide-isomerase and thioredoxin in catalysing disulphide isomerization in a protein substrate. Biochem. J. 275 (Pt 2), 349–353 (1991). [PubMed: 2025222]
33. Eschenlauer SCP & Page AP The Caenorhabditis elegans ERp60 homolog protein disulfide isomerase-3 has disulfide isomerase and transglutaminase-like cross-linking activity and is involved in the maintenance of body morphology. J. Biol. Chem. 278, 4227–4237 (2003). [PubMed: 12424233]
34. Smith CV, Jones DP, Guenthner TM, Lash LH & Lauterburg BH Compartmentation of glutathione: implications for the study of toxicity and disease. Toxicol. Appl. Pharmacol. 140, 1–12 (1996). [PubMed: 8806864]
35. Rubartelli A, Bajetto A, Allavena G, Wollman E & Sitia R Secretion of thioredoxin by normal and neoplastic cells through a leaderless secretory pathway. J. Biol. Chem. 267, 24161–24164 (1992). [PubMed: 1332947]
36. Dihazi H et al. Secretion of ERP57 is important for extracellular matrix accumulation and progression of renal fibrosis, and is an early sign of disease onset. J. Cell Sci. 126, 3649–3663 (2013). [PubMed: 23781031]
37. Pacello F, D'Orazio M & Battistoni A An ERp57-mediated disulphide exchange promotes the interaction between Burkholderia cenocepacia and epithelial respiratory cells. Sci. Rep. 6, 21140 (2016).
38. Lasecka L & Baron MD The nairovirus nairobi sheep disease virus/ganjam virus induces the translocation of protein disulphide isomerase-like oxidoreductases from the endoplasmic reticulum to the cell surface and the extracellular space. PLoS One 9, e94656 (2014).

39. Ott L et al. Evaluation of invertebrate infection models for pathogenic corynebacteria. FEMS Immunol. Med. Microbiol. 65, 413–421 (2012). [PubMed: 22443092]
40. Dunbar TL, Yan Z, Balla KM, Smelkinson MG & Troemel ERC elegans detects pathogen-induced translational inhibition to activate immune signaling. Cell Host Microbe 11, 375–386 (2012). [PubMed: 22520465]
41. Moskaug JO, Sandvig K & Olsnes S Cell-mediated reduction of the interfragment disulfide in nicked diphtheria toxin. A new system to study toxin entry at low pH. J. Biol. Chem. 262, 10339–10345 (1987). [PubMed: 3112141]
42. Patel PC et al. Scavenger receptors mediate cellular uptake of polyvalent oligonucleotide-functionalized gold nanoparticles. Bioconjug Chem. 21, 2250–2256 (2010). [PubMed: 21070003]
43. Karala A-R, Lappi A-K & Ruddock LW Modulation of an active-site cysteine pKa allows PDI to act as a catalyst of both disulfide bond formation and isomerization. J. Mol. Biol. 396, 883–892 (2010). [PubMed: 20026073]
44. Wu C et al. Thioredoxin 1-mediated post-translational modifications: reduction, transnitrosylation, denitrosylation, and related proteomics methodologies. Antioxid. Redox Signal. 15, 2565–2604 (2011). [PubMed: 21453190]
45. Futerman AH & van Meer G The cell biology of lysosomal storage disorders. Nat. Rev. Mol. Cell Biol. 5, 554–565 (2004). [PubMed: 15232573]
46. Olson OC & Joyce JA Cysteine cathepsin proteases: regulators of cancer progression and therapeutic response. Nat. Rev. Cancer 15, 712–729 (2015). [PubMed: 26597527]
47. Vassar R, Kovacs DM, Yan R & Wong PC The beta-secretase enzyme BACE in health and Alzheimer's disease: regulation, cell biology, function, and therapeutic potential. J. Neurosci. 29, 12787–12794 (2009). [PubMed: 19828790]
48. Seidah NG & Prat A The biology and therapeutic targeting of the proprotein convertases. Nat. Rev. Drug Discov. 11, 367–383 (2012). [PubMed: 22679642]
49. Nomura DK, Dix MM & Cravatt BF Activity-based protein profiling for biochemical pathway discovery in cancer. Nat. Rev. Cancer 10, 630–638 (2010). [PubMed: 20703252]
50. Prifti E et al. A fluorogenic probe for SNAP-tagged plasma membrane proteins based on the solvatochromic molecule Nile Red. ACS Chem. Biol. 9, 606–612 (2014). [PubMed: 24471525]

Reference for Methods.

1. Presolski SI, Hong VP & Finn MG Copper-Catalyzed Azide-Alkyne Click Chemistry for Bioconjugation. Curr Protoc Chem Biol 3, 153–162 (2011). [PubMed: 22844652]
2. Bhatia D, Surana S, Chakraborty S, Koushika SP & Krishnan Y A synthetic icosahedral DNA-based host-cargo complex for functional in vivo imaging. Nat Commun 2, 339 (2011). [PubMed: 21654639]
3. Altschul SF, Gish W, Miller W, Myers EW & Lipman DJ Basic local alignment search tool. JMolBiol 215, 403–410 (1990).
4. Kamath RS & Ahringer J Genome-wide RNAi screening in Caenorhabditis elegans. Methods 30, 313–321 (2003). [PubMed: 12828945]
5. Rual J-F et al. Toward improving Caenorhabditis elegans phenome mapping with an ORFeome-based RNAi library. Genome Res 14, 2162–2168 (2004). [PubMed: 15489339]
6. Dunbar TL, Yan Z, Balla KM, Smelkinson MG & Troemel ERC elegans detects pathogen-induced translational inhibition to activate immune signaling. Cell Host Microbe 11, 375–386 (2012). [PubMed: 22520465]
7. Xu D, Perez RE, Rezaiekhaligh MH, Bourdi M & Truog WE Knockdown of ERp57 increases BiP/GRP78 induction and protects against hyperoxia and tunicamycin-induced apoptosis. Am J Physiol Lung Cell Mol Physiol 297, L44–51 (2009). [PubMed: 19411306]

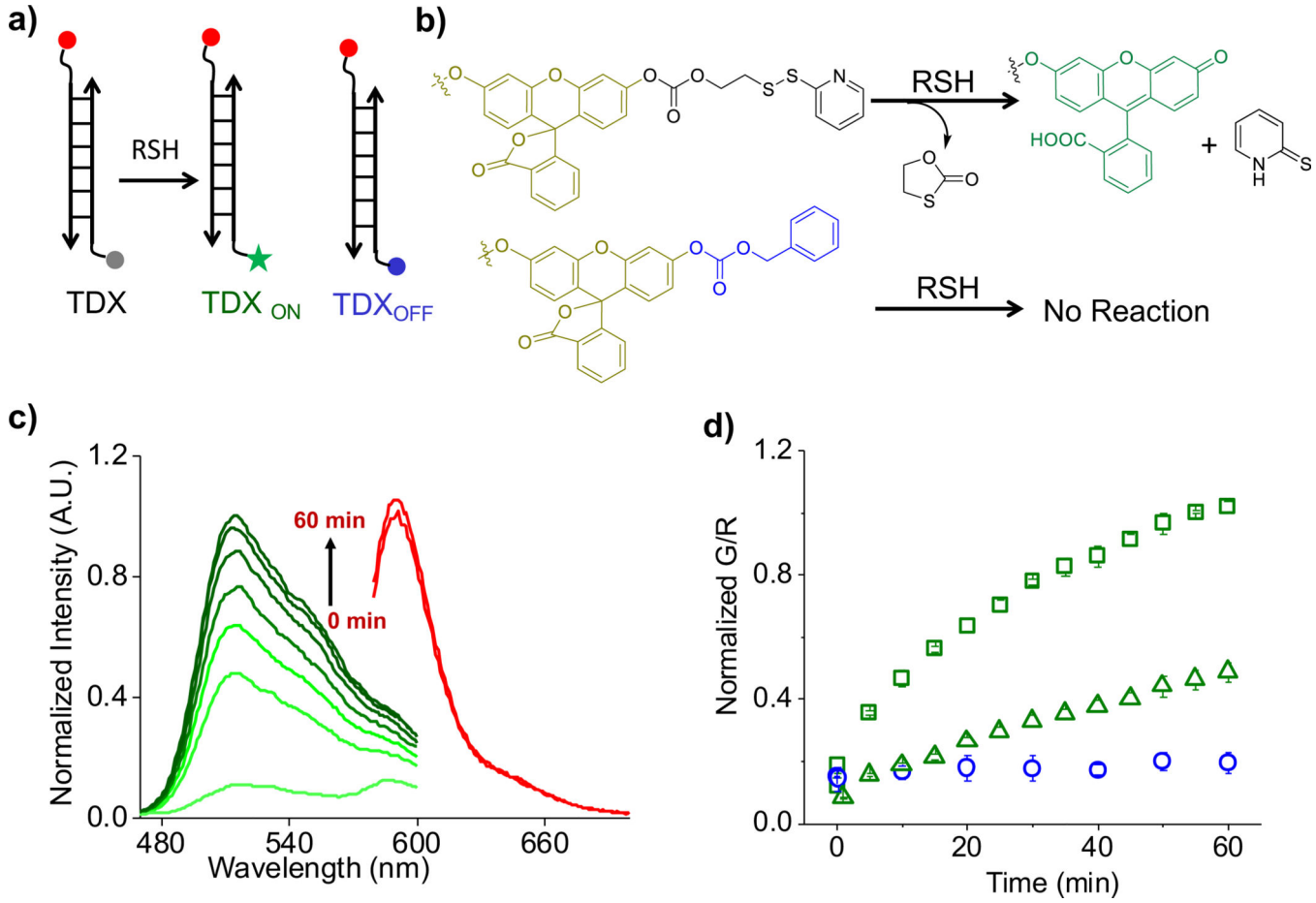

Figure 1: Design and *in vitro* Characterization of TDX reporter.

a) Structure of the TDX reporter (left): the sensing module (grey) is a caged fluorescein dye conjugated with a disulfide moiety, the normalizing module (red) is a thiol-insensitive rhodamine fluorophore, and the targeting module is a DNA duplex (black lines). The reporter (TDX) undergoes thiol disulfide exchange to give highly fluorescent TDX_{ON}. TDX_{OFF} (right) is a constitutively off version of TDX where fluorescein is caged by a benzyloxycarbonate group non-responsive to thiols (blue). **b)** Working principle of sensing module of TDX in presence of reduced thiols. **c)** Fluorescence emission spectra of sensing module (green, G) and normalizing module (red, R) of TDX in 5 mM glutathione at pH=7.2 as a function of time. **d)** Ratio of fluorescence intensities (G/R) of TDX_{OFF} (blue open circle, pH=7.2) and TDX in presence of 5 mM glutathione as a function of time at pH=7.2 (green, open square), pH=6.0 (green, open triangle). Error bar indicates the mean of three independent experiments ± s.e.m

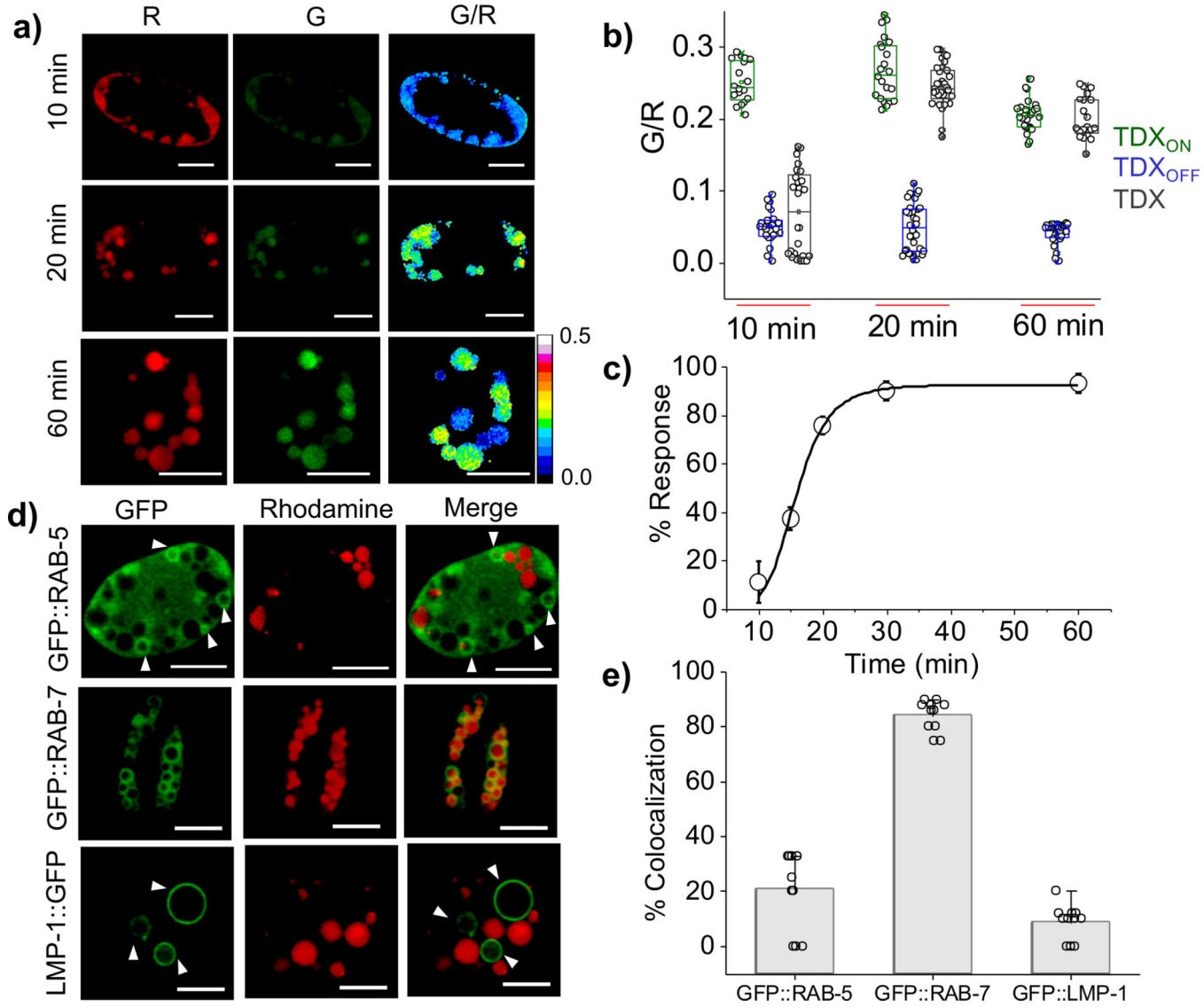

Figure 2: Spatiotemporal detection of thiol disulfide exchange reaction in endo-lysosomal compartment of *C. elegans* coelomocytes.

a) Representative pseudo-colored images of TDX reporter's endocytosed by coelomocytes at indicated time points post injection. **b)** Box plot showing G/R ratio at different time points (n = 20 cells, ≥ 80 endosome). **c)** Plot of percentage (%) response of TDX reporter at different time point post injection in worms, Error bar indicates the mean of three independent experiments ± s.e.m. **d)** Colocalization of TDX^R with transgenic worms expressing molecular markers of endocytic vesicles such as GFP::RAB-5, GFP::RAB-7 and LMP-1::GFP in coelomocytes, 20 min post injection (n = 10 cells, ≥ 50 endosomes). Scale bar, 5 μm. **e)** Quantification of colocalization in **(d)**.

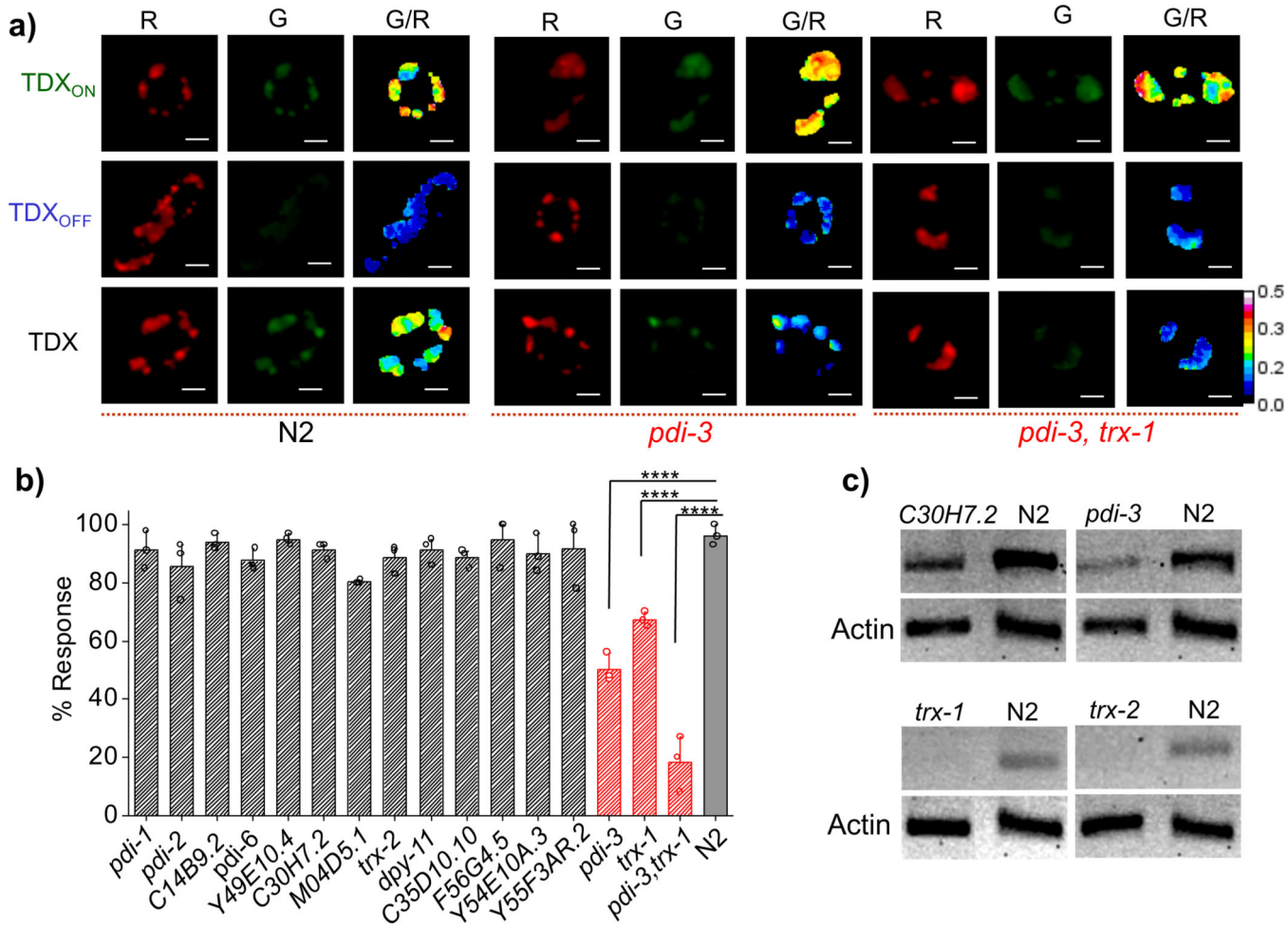

Figure 3: PDI-3 and TRX-1 are responsible for disulfide exchange reaction inside endocytic vesicles.

a) Representative pseudo-color images of coelomocytes labeled individually with TDX$_{ON}$, TDX$_{OFF}$ and TDX in worms of indicated genetic backgrounds. **b)** Plot of % response of TDX in different mutants and RNAi knockdowns 20 min post injection. Error bars indicate the mean of three independent experiments ± s.e.m. (n = 10 cells, ≥ 50 endosomes). **** indicates the two tailed *p* value is less than 0.0001 in unpaired t test, % response of *pdi-3, trx-1* and *pdi-3, trx-1* double RNAi worms at 20 min post injection. c) RT-PCR analysis of total RNA isolated from wild type (N2) and RNAi worms. PCR amplified cDNA of specified gene products in both RNAi and N2 worms are shown. Actin is used as a loading control. Scale bar, 5 μm.

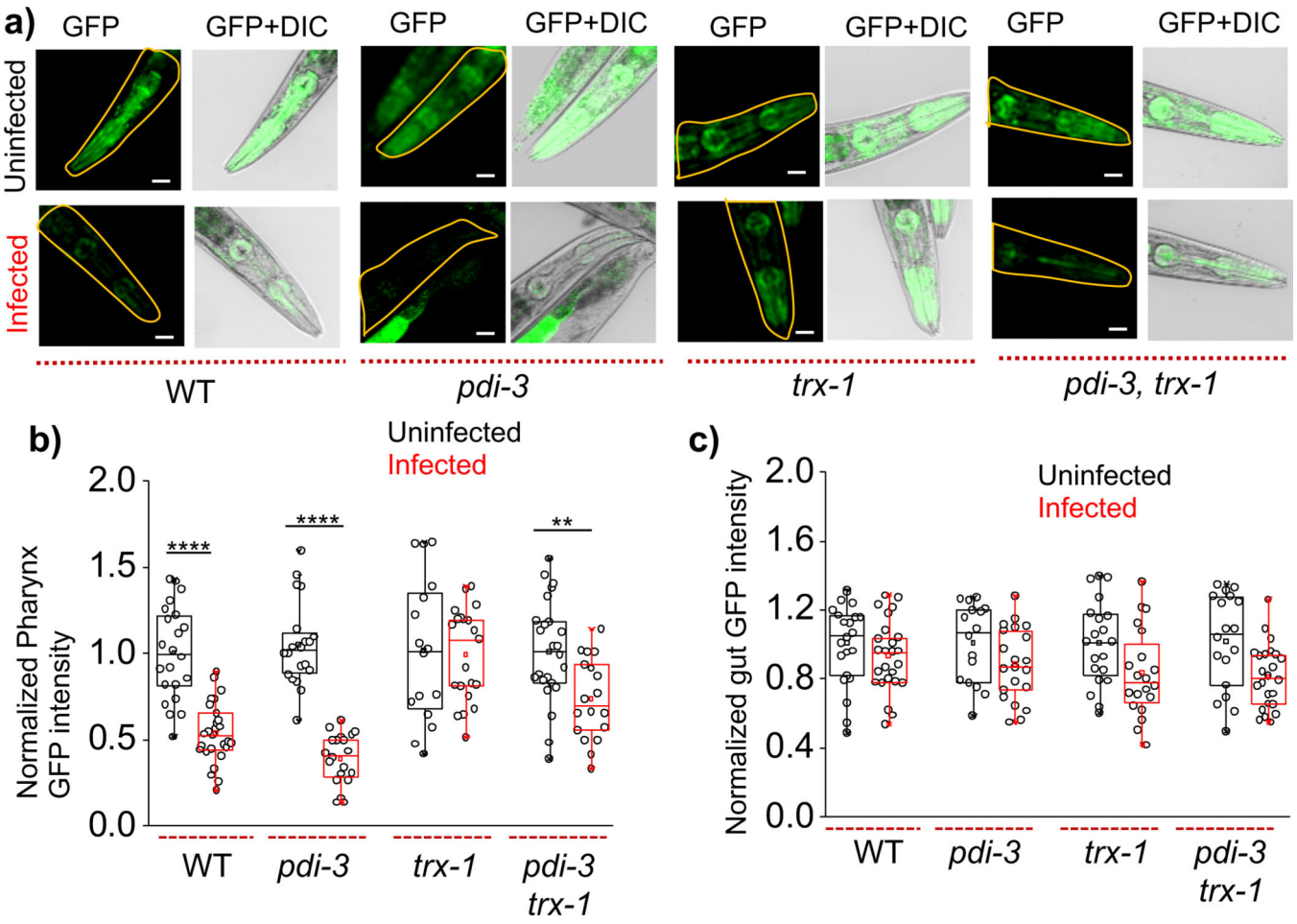

Figure 4: Thioredoxin-1 offers protection against DT infection.

a) Representative pseudo-color and overlaid images of pharyngeal GFP expression in indicated genetic backgrounds of nematodes infected or not infected with *C. diphtheriae.* Box plots of normalized **b)** pharyngeal and **c)** intestinal GFP intensity of infected and non-infected nematodes with indicated genetic background (n = 20 worms). GFP intensity distribution is normalized by mean intensity of respective not infected worm. ****p <0.0001 and **$p < 0.005$ obtained using unpaired t-test. Scale bar, 100 μm. Experiments are replicated in duplicates.

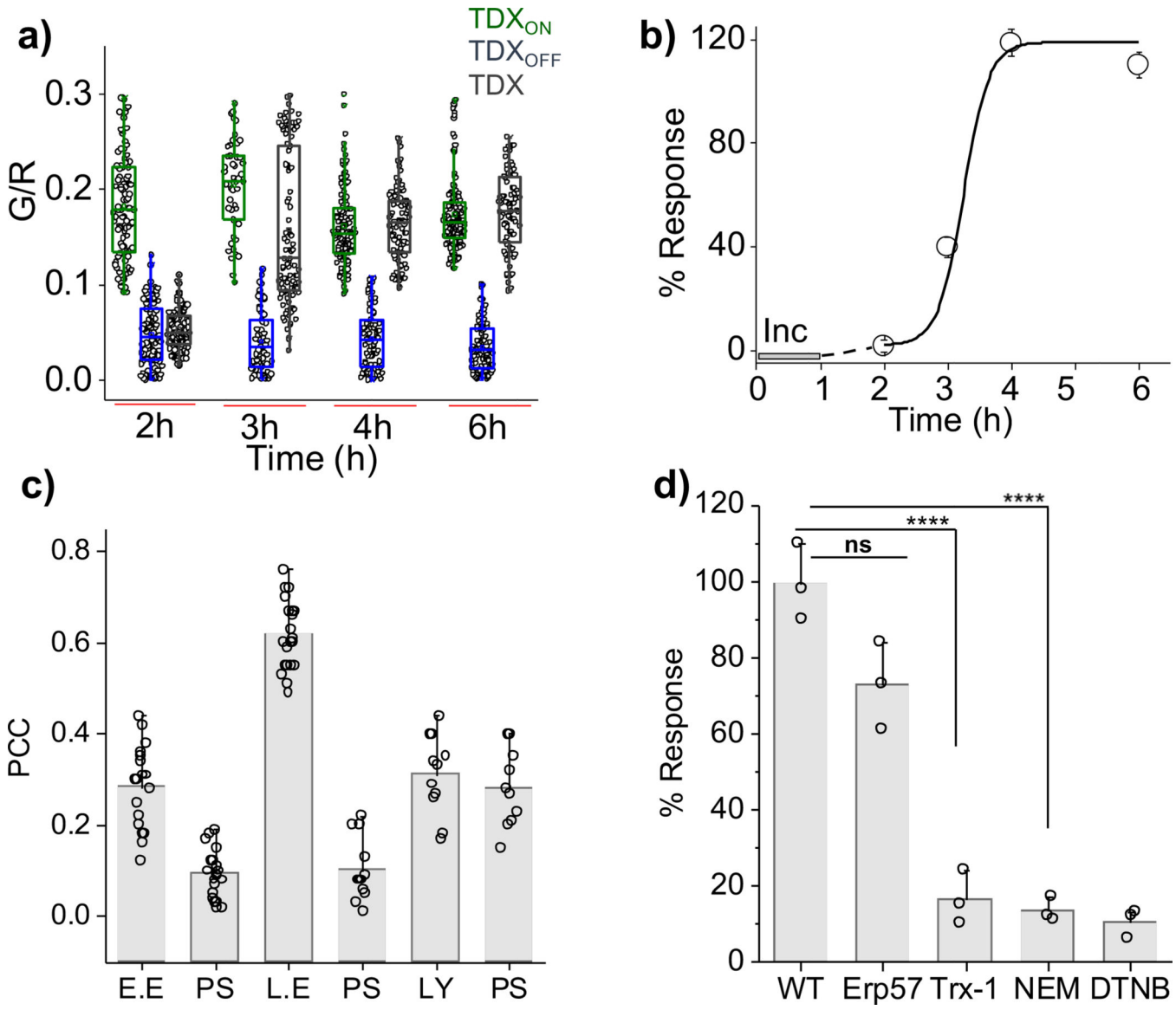

Figure 5: TRX-1 mediates endosomal disulfide reduction in mammalian cells.

a) Box plot of G/R values of the TDX reporter system in HeLa cells at indicated time points post internalization (n = 20 cells, ≥150 endosomes). b) Percentage (%) response of the TDX reporter system as a function of time, [Inc. = incubation period, line serves as a visual aid]. c) Pearson's correlation coefficient (PCC) of colocalization between pulsed TDX_{A647} after a 3 h chase in HeLa cells expressing endosomal markers. [E.E. = early endosome, Rab5-RFP, L.E. = late endosome, Rab7-RFP), Ly = lysosome, TMR dextran, PS = pixel shift] (n ≥ 10 cells), d) Percentage (%) response of the TDX reporter system at t = 4 h in HeLa cells treated with indicated inhibitors or siRNAs against indicated proteins, [NEM = N-ethyl maleimide, DTNB = 5, 5-dithio-bis-(2-nitrobenzoic acid)]. Error bar corresponds to s.e.m. from three independent experiment, ns = not significant, **** p <0.0001 obtained using unpaired t-test.